Letter Vol. 51, No. 16 / 15 August 2026 / Optics Letters 4677



Fully passive quantum bits encoding scheme based on dual-laser interference

Zhao-Yuan Chen,* Yan-Fei Liu, Zhi-Li Zhang, Xiao-Sheng Si, Yang Gao, Hao Zheng, Tian-Mei Li, and Lei Feng

Xi'an Research Institute of High Technology, Xi'an 710025, China
**fl130472@mail.ustc.edu.cn*

Received 3 June 2026; revised 3 August 2026; accepted 3 August 2026; posted 4 August 2026; published 13 August 2026

This Letter presents a transmitter-side fully passive QKD encoding scheme based on dual-laser interference, eliminating delay-line structures and active modulation components. Two independent laser diodes are precisely controlled in time and frequency domains to achieve consistent pulse timing, intensity, and spectra. Experimental interference results agree well with theoretical intensity distributions. Numerical simulations using the FP-QKD protocol based on a dual-laser passive encoding source show secure key extraction over distances exceeding 100 km with a 10^{12} block size, and an SKR above 10^5 bits/s for short distances. The scheme offers improved stability and significantly higher encoding rates compared to prior implementations. © 2026 Optica Publishing Group. All rights, including for text and data mining (TDM), Artificial Intelligence (AI) training, and similar technologies, are reserved.

https://doi.org/10.1364/OL.607148

Introduction. Quantum key distribution (QKD) enables secure key exchange between users by harnessing the fundamental principles of quantum mechanics, making it a vital technology for protecting communications in the quantum information era [1]. In recent years, QKD research has advanced significantly, with ongoing efforts focused on enhancing both the security and practicality of the systems [2,3]. Measurement-device-independent (MDI) and twin-field (TF) protocols, for example, effectively remove side-channel vulnerabilities at the receiver end [4–8]. All these QKD systems require a quantum state preparation stage. Practical device imperfections often cause implementations to deviate from the theoretical ideal, creating potential loopholes for eavesdroppers [9–15].

To mitigate such risks, fully passive (FP) QKD schemes have been introduced [16–24]. This scheme passively encodes quantum bits by utilizing the random phase inherent in weak coherent pulses, eliminating the need for active modulation components and thus inherently resisting Trojan-horse attacks. Recent work by Gnanapandithan *et al.* on hidden multidimensional modulation side channels in QKD systems further highlights the security benefits offered by FP-QKD architecture [25]. Furthermore, FP-QKD operates without active modulators, thereby removing the need for the complex and power-consuming driving circuits typically associated with them. The randomness required for encoding originates directly from the inherent phase randomness of gain-switched laser pulses, which effectively integrates a quantum random number generator into the photon source. This leads to a significantly simplified system architecture. These attributes provide substantial advantages for the practical implementation and deployment of this technology.

Currently, experimental implementations of FP-QKD have predominantly adopted an optical design based on a single laser followed by a delay-line structure. In this scheme, four adjacent laser pulses in the time domain are delayed separately and then made to interfere with one another for encoding. This approach avoids wavelength mismatch issues that arise when multiple lasers are used and enables high-quality interference. However, it also introduces several practical limitations. First, the scheme generates redundant, non-encoded optical pulses, which must be filtered out by additional optical switches or accounted for within the security analysis [26] to prevent information leakage. As noted by Wang *et al.* [18], ensuring security typically requires at least two optical switches with an extinction ratio exceeding 30 dB. Although these switches are driven by fixed periodic signals—and thus are not vulnerable to Trojan-horse attacks—they still introduce active modulation components and driving circuits into the system, thereby increasing its complexity. Second, the lengths of the delay lines on both Alice's and Bob's sides must be precisely controlled to maintain optimal interference. In practice, these paths are usually constructed using fused fiber components, whose lengths are difficult to adjust once configured. Any change in the system clock frequency would therefore necessitate rebuilding the entire encoding optical setup. Third, the scheme exhibits low utilization efficiency of laser pulses. For example, in the experiment conducted by Lu *et al.* [19], while the pulse repetition rate was 200 MHz, the encoded bit rate after delayed interference was only 50 MHz, leading to a low encoding rate.

In this Letter, we propose a simplified FP encoding scheme. This approach utilizes interference between laser pulses generated by two individual laser diodes (LDs), thereby avoiding the need for a delay-line structure. By employing a time-bin encoding method, it also eliminates the requirement for additional optical switches. Furthermore, a symmetric filtering optical path is designed to mitigate wavelength mismatch between different LDs.

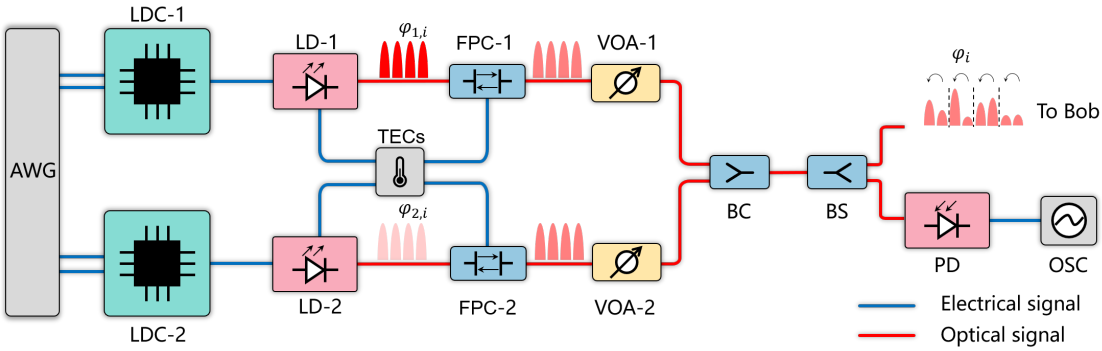


Fig. 1. Experimental setup. AWG, arbitrary waveform generator (Keysight 81134A); BC, beam combiner; BS, beam splitter; FPC, Fabry–Pérot cavity; LD, laser diode with 1550 nm wavelength; LDC, self-developed laser driver chip; OSC, oscilloscope (DSA-X 91604A); PD, photodetector (Newport 1544B); TEC, thermoelectric coolers; VOA, variable optical attenuator. The blue and red lines represent electrical and optical signals, respectively.

Experimental setup. Figure 1 illustrates the structure of the proposed dual-laser interference encoding scheme. An arbitrary waveform generator (AWG) provides two channels of periodic differential signals as input to the laser driver chips (LDCs) [27]. LDCs drive two LDs in gain-switch mode to generate laser pulse sequences. The laser beams are then filtered and attenuated by a Fabry–Pérot cavity (FPC) and a variable optical attenuator (VOA) to ensure that the spectrum and intensity of the two laser pulses are consistent. Subsequently, two laser beams interfere at a beam combiner (BC) to complete bit encoding. After being split by a beam splitter (BS), one part is sent to Bob, while the other part is used for local measurement. In the local measurement part, we use a photodetector (PD) to detect the intensity of the interfered laser pulses, and an oscilloscope to record the laser pulse signals. Furthermore, the LDs and FPCs are temperature-stabilized via thermoelectric coolers (TECs) to suppress wavelength drift caused by environmental temperature fluctuations [28].

The AWG output signals have a repetition rate of 1 GHz to achieve higher encoding rates of 500 MHz. The driving signals for both channels originate from the same clock source of the AWG. Therefore, the relative jitter of the two driving signals in the time domain arises only from the noise of the subsequent circuits, which is very small and negligible. This enables precise temporal alignment of two laser pulses. To obtain optical pulses with completely random phases, we employ a narrow-pulse, high-amplitude driving current, which rapidly depletes the population inversion inside the laser diode, achieving complete turn-off of oscillation and thus complete phase independence between pulses. Theoretically, the laser pulse phases $\varphi_{1,i}$ and $\varphi_{2,i}$ of LD-1 and LD-2 are independent and uniformly distributed variables, $\varphi_{1,i}, \varphi_{2,i} \sim \mathrm{U}(0, 2\pi)$. Therefore, the intensity μ of the laser pulses after interference follows a U-shaped distribution with probability density function $p(\mu) = \frac{1}{\pi\sqrt{\mu(\mu_m - \mu)}}$, where $\mu_m = 4\nu$ is the maximum intensity after interference, and ν is the average intensity of each pulse. The phase of interference pulse is $\varphi_i = (\varphi_{1,i} + \varphi_{2,i})/2$, which also follows a uniform distribution $\mathrm{U}(0, 2\pi)$. Two adjacent pulses after interference are combined to form a qubit. The intensity of two consecutive bins serves as the Z basis, while the phase difference between two bins serves as the X basis. Since the intensity and phase of each encoded pulse are independent and random, a qubit formed by combining two pulses can traverse the entire encoding space. In a complete FP-QKD system, Alice requires a local measurement module to characterize each generated qubit. For each qubit, Alice's local measurement obtains the per-bin intensities and the inter-bin phase difference. Based on these measurement results, post-selection is performed to determine basis assignment, bit value, and decoy-state region. The complete encoding and post-selection protocol is provided in Supplement 1.

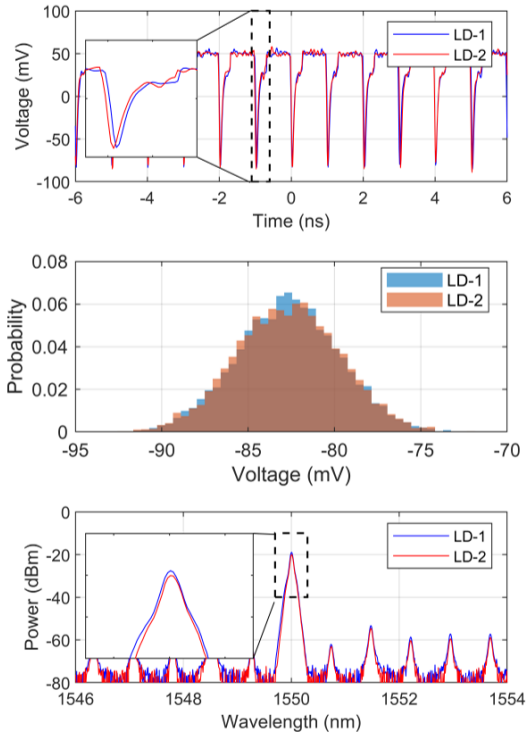


Fig. 2. Characterization of two lasers before interference. (a) Temporal waveforms; (b) pulse peak statistical distribution; and (c) filtered optical spectra.

Results. Figure 2 presents the experimental test results for consistency control of two LDs. Figure 2(a) compares the temporal waveforms of two LDs, demonstrating excellent temporal alignment between the two pulse sequences. The enlarged inset highlights a set of pulses with relatively larger timing jitter. Even for these pulses, the timing jitter remains approximately 20 ps, which is well within the acceptable range for high-visibility interference. This precise synchronization is a direct consequence

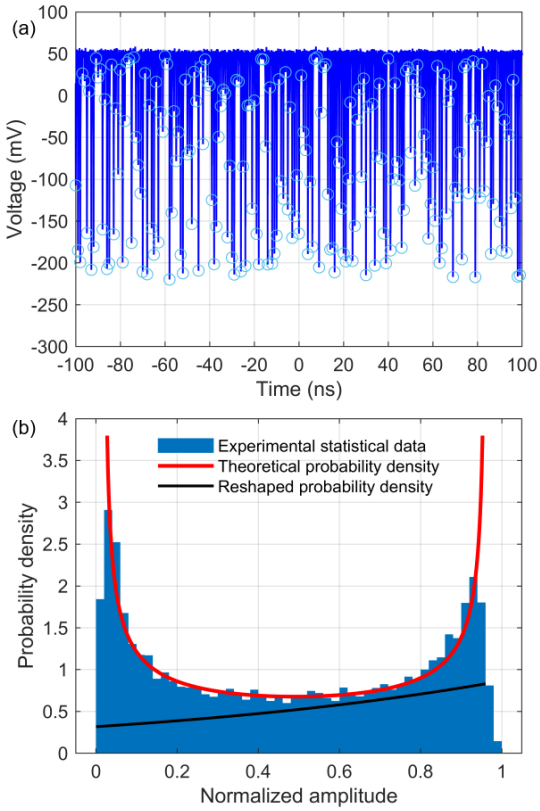


Fig. 3. Interference results of two lasers. (a) Waveform and amplitude of the pulses after interference. (b) The blue histogram shows the statistical results of the pulse amplitude after interference; the red line represents the theoretical probability density distribution of the pulse amplitude after interference; the black line represents the probability density after post-selection reshaping.

of driving both LDs from the same clock source of the AWG, as described in the experimental setup.

Figure 2(b) shows the histograms of the peak intensity distributions for both LDs. Two distributions exhibit substantial overlap, with the mean intensity difference measured to be less than 3% of the average peak value. This intensity matching is essential for maintaining high interference visibility, as any imbalance directly reduces the modulation depth of the interfered pulses. The observed consistency is achieved through careful adjustment of the VOAs and the symmetric optical path design.

Figure 2(c) displays a comparison of the optical spectra from two lasers, with the spectral peak region shown in detail. Both spectra are centered at approximately 1550.014 nm, and the line shapes of the two spectra show excellent agreement. In addition to the main peak, multiple secondary peaks are also observed in the spectra, which originate from the filtering effect of the FPC.

The spectral consistency ensures that two lasers operate at the same central wavelength with comparable spectral properties. These experimental results demonstrate that two laser pulses exhibit good consistency across all key parameters, including temporal alignment, peak intensity, and spectral characteristics, laying the foundation for high-quality interference.

Figure 3 presents the experimental results of the interference. (a) Shows the interference waveform along with the peak detection results, where the interference pattern exhibits random intensity fluctuations that are characteristic of the random

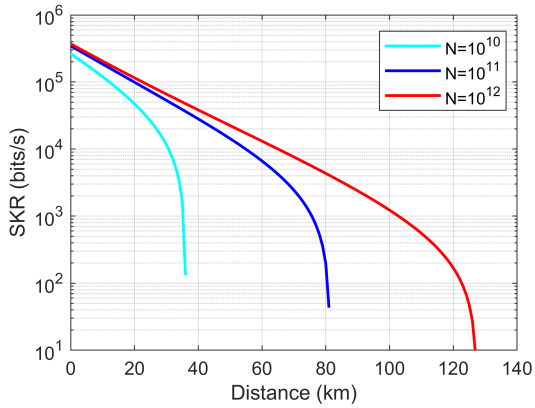


Fig. 4. Simulated secure key rate (SKR) for block sizes of 10^{10}, 10^{11}, and 10^{12} (cyan, blue, and red lines, respectively).

encoding scheme. (b) Displays the statistical distribution of the pulse amplitude compared with the theoretically calculated probability density function. The experimental data show good agreement with the theoretical prediction, confirming that the proposed scheme can achieve fully passive random encoding.

However, slight deviations between the experimental statistics and the theoretical curve are observed. These can be attributed to several practical factors. First, the noise from the PD and oscilloscope introduces background fluctuations that affect the measurement accuracy, especially for low-amplitude pulses. Second, the intensity differences between two laser pulses result in non-ideal interference visibility, which slightly distorts the statistical distribution from the ideal U-shape toward a more flattened shape. Third, environmental instabilities such as temperature fluctuations and mechanical vibrations may cause slow drift in the relative phase and intensity over the measurement time. Despite these minor deviations, the overall agreement between experiment and theory validates the effectiveness of the dual-laser interference encoding approach. Furthermore, we employ the method of reshaping the probability density function from Ref. [18] to perform post-selection on the encoded bits, as shown by the black line in Fig. 3(b). The post-selection process discards a fraction of the encoded bits that fall outside a predefined window. This operation not only decouples the intensity state from the time-bin state, but also ensures that the probability density function of the remaining qubits follows an ideal exponential distribution. As a result, the probability distribution after post-selection is not affected by the aforementioned non-ideal factors, ensuring that the subsequent security analysis can be based on the ideal theoretical model.

To evaluate the practical performance of the proposed dual-laser interference encoding scheme, we simulate the secure key rate (SKR) as a function of transmission distance using the FP-QKD protocol [18]. The pulse clock rate is 1 GHz. Using the post-selection method shown by the black line in Fig. 3(b), we reconstruct the probability density of the encoded qubits. Incorporating the finite-key size effect into parameter estimation [24,29–31], the simulated SKR results are presented in Fig. 4 (details in Supplement 1). Simulations indicate that with a block size of 10^{12} transmission rounds, the proposed scheme enables key extraction over distances greater than 100 km. For short-distance communication, the SKR can exceed 10^5 bits/s. It is worth noting that the high secure key rate at short distances can be achieved with a block size of only 10^{10}

transmission rounds, corresponding to an accumulation time of about 20 s. This suggests that the FP-QKD scheme is more suitable for short-distance, lightweight applications. Therefore, the proposed scheme—offering reduced system complexity and lower environmental sensitivity—is better aligned with such scenarios.

Conclusion and discussion. In this study, we propose a transmitter-side fully passive quantum bit encoding scheme based on dual-laser interference. The key innovation lies in replacing conventional delay-line structures and active modulation components with a simple dual-laser interference architecture. To ensure reliable operation of two independent laser diodes, we develop time-domain and frequency-domain parameter control techniques that achieve excellent consistency in pulse timing, intensity, and spectral properties. Experimental results are in excellent agreement with theoretical calculations, confirming the feasibility of the dual-laser interference approach for QKD applications. Based on this encoding scheme, we further simulate the SKR using the FP-QKD protocol. The results show that key extraction over distances exceeding 100 km is achievable. The significance of this work lies in its substantial simplification of FP-QKD systems. By eliminating the delay-line structure and active modulation components, the proposed scheme offers significantly improved system stability and robustness against environmental perturbations. Furthermore, the encoding rate reaches 500 MHz, representing a major advancement over previous experimental implementations that achieved only tens of megahertz in encoded bit rates.

The cornerstone of our approach is maintaining consistency between the parameters of the two lasers. Such consistency is essential for guaranteeing the effectiveness of the interference encoding and the overall system security. During prolonged system operation, factors such as thermal accumulation in the devices and ambient temperature variations may affect the interference outcome, potentially leading to information leakage. Several strategies can mitigate this concern. On the practical side, a feedback control loop can be employed: by monitoring the real-time output state distribution of the passive transmitter, systematic deviations can be detected and corrected through a temperature controller and driving current. On the theoretical side, a quantitative model can be established linking the degree of laser parameter mismatch to the amount of potential information leakage, allowing the key extraction formula to be appropriately modified to account for residual distinguishability and thereby reduce the security risk.

Future work will focus on two main directions. First, a complete, fully passive QKD system incorporating a receiver, single-photon detector [32,33], local monitoring, synchronization, and real-time post-processing remains the subject of future work. This would enable real-time QKD and systematic validation of system performance under practical conditions, including long-term stability tests and finite-key analysis. Experimental characterization of the SKR over various fiber distances would provide direct verification of the simulation results. Second, the encoding scheme can be implemented on a silicon photonic chip platform. Using silicon photonics technology, all optical components can be integrated onto a single chip, dramatically improving system integration, reducing footprint and power consumption, and eliminating temperature sensitivity. Chip-scale integration also promises lower production costs and mass production capability, paving the way for compact and scalable FP-QKD transmitters for future quantum networks.

Funding. Shaanxi Science and Technology Department (2025JC-YBQN-043, 2025JC-YBMS-677); National Natural Science Foundation of China (62274182, 62450056).

Acknowledgment. The authors gratefully acknowledge the University of Science and Technology of China for technical support and Xin-Zhe Wang for providing the LDCs.

Disclosures. The authors declare no conflicts of interest.

Data availability. Data underlying the results presented in this paper are not publicly available at this time but may be obtained from the authors upon reasonable request.

Supplemental document. See Supplement 1 for supporting content.

REFERENCES

1. N. Gisin, G. Ribordy, W. Tittel, *et al.*, Rev. Mod. Phys. **74**, 145 (2002).
2. F. Xu, X. Ma, Q. Zhang, *et al.*, Rev. Mod. Phys. **92**, 025002 (2020).
3. C. Y. Lu, Y. Cao, C. Z. Peng, *et al.*, Rev. Mod. Phys. **94**, 035001 (2022).
4. H. K. Lo, M. Curty, and B. Qi, Phys. Rev. Lett. **108**, 130503 (2012).
5. H. L. Yin, T. Y. Chen, Z. W. Yu, *et al.*, Phys. Rev. Lett. **117**, 190501 (2016).
6. M. Lucamarini, Z. L. Yuan, J. F. Dynes, *et al.*, Nature **557**, 400 (2018).
7. X. Zhong, J. Hu, M. Curty, *et al.*, Phys. Rev. Lett. **123**, 100506 (2019).
8. F. Ji, P. Huang, T. Wang, *et al.*, Photon. Res. **12**, 1485 (2024).
9. V. Scarani, H. Bechmann-Pasquinucci, N. J. Cerf, *et al.*, Rev. Mod. Phys. **81**, 1301 (2009).
10. F. Xu, B. Qi, and H.-K. Lo, New J. Phys. **12**, 113026 (2010).
11. S.-H. Sun, F. Xu, M.-S Jiang, *et al.*, Phys. Rev. A **92**, 022304 (2015).
12. H. Tan, M. Petrov, W. Zhang, *et al.*, Phys. Rev. X Quantum **6**, 040331 (2025).
13. F.-Y. Lu, Z.-H. Wang, Y. Zhou, *et al.*, Nat. Commun. **16**, 11487 (2025).
14. G.-J. Fan-Yuan, W.-X. Xie, D.-Y. He, *et al.*, Proc. Natl. Acad. Sci. U.S.A. **123**, e2521590123 (2026).
15. J.-X. Li, Y.-G. Shan, R. Wang, *et al.*, Sci. Adv. **12**, eaed2420 (2026).
16. M. Curty, X. Ma, B. Qi, *et al.*, Phys. Rev. A **81**, 022310 (2010).
17. M. Curty, X. Ma, H.-K. Lo, *et al.*, Phys. Rev. A **82**, 052325 (2010).
18. W. Wang, R. Wang, C. Hu, *et al.*, Phys. Rev. Lett. **130**, 220801 (2023).
19. F.-Y. Lu, Z.-H. Wang, J.-L. Chen, *et al.*, Phys. Rev. Lett. **131**, 110802 (2023).
20. C. Hu, W. Wang, K.-S. Chan, *et al.*, Phys. Rev. Lett. **131**, 110801 (2023).
21. J. Li, W. Wang, and H.-K. Lo, Phys. Rev. Appl. **21**, 064056 (2024).
22. X. Wang, F.-Y. Lu, Z.-H. Wang, *et al.*, Phys. Rev. Appl. **21**, 064067 (2024).
23. V. Zapatero, W. Wang, and M. Curty, Quantum Sci. Technol. **8**, 025014 (2023).
24. V. Zapatero and M. Curty, Phys. Rev. Appl. **21**, 014018 (2024).
25. A. Gnanapandithan, L. Qian, and H.-K. Lo, Phys. Rev. Lett. **134**, 130802 (2025).
26. Á. Navarrete, V. Zapatero, and M. Curty, NPJ Quantum Inf. **11**, 187 (2025).
27. Y. Zhu, X. Wang, C. Zhu, *et al.*, AIP Adv. **12**, 125025 (2022).
28. J.-L. Chen, D.-Y. He, Z.-H. Wang, *et al.*, Rev. Sci. Instrum. **95**, 063002 (2024).
29. C.-H. F. Fung, X. Ma, and H. F. Chau, Phys. Rev. A **81**, 012318 (2010).
30. C. C. W. Lim, M. Curty, N. Walenta, *et al.*, Phys. Rev. A **89**, 022307 (2014).
31. M. Tomamichel and A. Leverrier, Quantum **1**, 14 (2017).
32. J.-L. Chen, D.-Y. He, S. Wang, *et al.*, Photonics Res. **12**, 3027 (2024).
33. D.-Y. He, S. Wang, J.-L. Chen, *et al.*, Adv. Devices Instrum. **4**, 0020 (2023).